Interface based damage-plasticity model for predicting the compressive failure of masonry under monotonic and cyclic loads

Yu Nie, Abdul Sheikh, Michael Griffith, Phillip Visintin and Jaroslav Vaculik

School of Civil, Environmental and Mining Engineering, University of Adelaide, SA 5000, Australia

Abstract

In this paper, the compressive behaviour of masonry structures is predicted by proposed interfacial constitutive model which contains plasticity and damage mechanism to model the nonlinear response of masonry mortar joints. The interfacial model has an elliptical yield surface in the plasticity framework and its hardening/softening strength along the variation of plastic energy dissipation is controlled by the damage parameter. Based on the traction-separation law, the proposed interfacial model is defined into the cohesive element in the finite element model to simulate the compressive of masonry under both monotonic and cyclic compressive loading conditions. Compared with plasticity models and pure damage models, the proposed damage-plasticity model can better simulate the response of masonry in terms of its stiffness degradation and inelastic deformation. The unloading-reloading mechanical characteristics of masonry structures is modelled by the interface model which has well consistency with experimental results from literature.

Keywords: masonry simulation, finite element modelling, interface constitutive model

1 Introduction

Masonry structures, which are widely used in residential and public buildings, are especially vulnerable to cyclic loads when earthquake occurs. Based on the research reported by Ingham and Griffith (2011), the vast majority of damage was happen in unreinforced brick masonry (URM) buildings in the 2010 Christchurch earthquake. In recent years, the prediction of cyclic response for masonry structures has aroused widespread interest in seismic engineering (Griffith et.al, 2007; Derakhshan et.al, 2013; Vaculik and Griffith et.al, 2018) in terms of the macro-behaviour of masonry structures by using analytical models. Similar macro concepts are adopted by studies (Milani et.al, 2007; Di Nino and Luongo, 2019) focus on numerical techniques which aim to simulate masonry structures by homogenising bricks and mortar joints into a continuum solid which is called representative volume element (RVE). Although the homogenisation approach has advantages with regard to computational efficiency and the accuracy of load-displacement response, it is limited in predicting the failure modes and post-failure deformation of masonry structures, which is vital in providing guideline for the masonry retrofitting (Su et.al, 2011; Burton et.al, 2021).

Detailed micro-modelling method (Sarhosis and Lemos, 2018; Greco et.al, 2020; Calderón et.al, 2019; Andreotti et.al, 2018) is another modelling strategy which include all components in the model, including the brick, mortar and the interface between brick-mortar. This modelling

approach can simulate precisely the cracking patterns and their propagation in mortar joints and bricks. However, the application of this approach is restrained in small size structures (such as masonry couplets or prisms) as well as simply loading conditions (monotonic load within small deformation) due to its extremely high computation costs. Therefore, a more practical modelling strategy, which is called simplified micro-method (Lotfi and Shing, 1994; Lourenço and Rots, 1997), is commonly accepted in simulating the real size masonry structures under complex loading conditions (Minga et.al, 2018; D'Altri et.al, 2019; Tubaldi et.al, 2020). The mortar joint in the simplified micro-model is lumped into an interface/cohesive element which represents all nonlinear response of the masonry while the bricks are simulated by using solid elements. In this way, both computational efficiency and modelling accuracy of the finite element (FE) models are considered, and this simplified method is also extended to the application of discrete element models (Bui et.al, 2021) and finite discrete element models (Smoljanović et.al, 2018).

In previous studies related to simplified micro-modelling (Lotfi and Shing, 1994; D'Altri et.al, 2019), the compressive behaviour in the interface model is often ignored and assuming the compressive failure is all subjected to brick elements having nonlinear continuum constitutive behaviour, which reduces the computational efficiency since finer meshing is required for solid elements. Therefore, in this study the compressive behaviour of masonry is investigated and simulated by using an interface based model within damage-plasticity framework.

2 Constitutive model

The interface based constitutive model, as shown in Figure 1, follows the traction-separation law behaviour in a 2D space where 'n' and 's' denote the normal and shear directions respectively. The elastic behaviour of the interface can be represented by Eq.(1) with the elastic stiffness matrix $[K^0]$, nominal stress vector $\{\sigma\}$ and relative displacement vector $\{u\}$.

$$\{\sigma\} = [K^0]\{u\}; \qquad \begin{Bmatrix}\sigma_n \\ \sigma_s\end{Bmatrix} = \begin{bmatrix}K_n^0 & 0 \\ 0 & K_s^0\end{bmatrix}\begin{Bmatrix}u_n \\ u_s\end{Bmatrix} \tag{1}$$

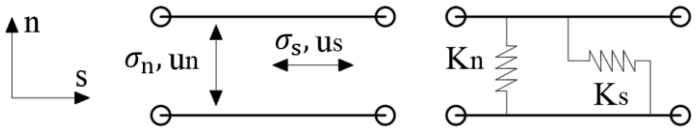

Figure 1 Elastic behaviour of the interface in 2D space

To define the strength/stiffness softening behaviour of mortar joints, a damage matrix $[D]$ is induced for the transformation between nominal stress $\{\sigma\}$ and effective stress $\{\bar{\sigma}\}$.

$$\{\sigma\} = ([I] - [D])\{\bar{\sigma}\}; \qquad \begin{Bmatrix}\sigma_n \\ \sigma_s\end{Bmatrix} = \begin{bmatrix}1 - D_n & 0 \\ 0 & 1 - D_s\end{bmatrix}\begin{Bmatrix}\bar{\sigma}_n \\ \bar{\sigma}_s\end{Bmatrix} \tag{2}$$

where $[I]$ is the unit matrix.

2.1 Yield surface

An elliptical yield surface (Figure 2) is adopted here to determine the elastic domain, which can be written as:

$$F_c\left(\{\bar{\sigma}\}, W_c^p\right) = C_{nn}\bar{\sigma}_n^2 + C_{ss}\bar{\sigma}_s^2 + C_n\bar{\sigma}_n - \left(f_c(W_c^p)\right)^2 \quad (3)$$

where C_{nn} and C_{ss} are parameters for controlling the configuration of the yield surface in normal and shear directions, and C_n is used to adjust the central position of the ellipse. W_c^p is the plastic work of the interface under compression and its increment can be calculated as:

$$dW_c^p = \left|\bar{\sigma}_n du_n^p\right| + \left|\bar{\sigma}_s du_s^p\right| \quad (4)$$

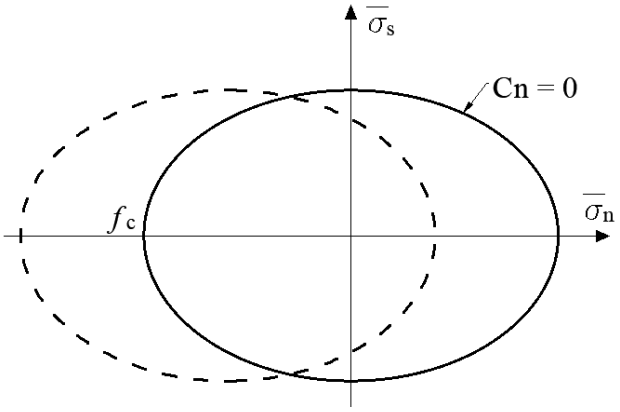

Figure 2 Yield surface of the compressive cap

The incremental plastic displacement $\{du^p\} = \begin{Bmatrix} du_n^p \\ du_s^p \end{Bmatrix}$ in current model is computed based on the associated flow rule, namely, potential surface is the same as yield surface, $Q_c = F_c$.

$$\{du^p\} = d\lambda \frac{\partial Q_c}{\partial\{\bar{\sigma}\}} = d\lambda \frac{\partial F_c}{\partial\{\bar{\sigma}\}} \quad (5)$$

where $d\lambda$ is the increment of plastic multiplier.

2.2 Damage parameter and strength evolution

Typically, the compressive failure of masonry prism includes hardening and softening behaviours in terms of the variation of compressive strength f_c along with the plastic work (or equivalent displacement). For the sake of numerical implementation by using damage parameters, in some literature (Minga et.al, 2018) the hardening component is ignored and only softening behaviour remained, as shown in Figure 3a. In this study, the hardening evolution is considered incorporating with the softening response (Figure 3b) which is determined by a damage parameter D_c.

In the Figure 3b, the strength evolution can be expressed by using a piecewise function:

$$f_c = \begin{cases} f_{ci} + (f_{cu} - f_{ci})\left(\dfrac{2W_c^p}{G_{fch}} - \left(\dfrac{W_c^p}{G_{fch}}\right)^2\right), & W_c^p \le G_{fch} \\ f_{cu} - (f_{cu} - f_{cr})\left[\alpha\left(\dfrac{W_c^p - G_{fch}}{G_{fcs}}\right)^{\alpha-1} - (\alpha-1)\left(\dfrac{W_c^p - G_{fch}}{G_{fcs}}\right)^{\alpha}\right], & G_{fch} < W_c^p \le G_{fc} \\ f_{cr}, & W_c^p > G_{fc} \end{cases} \quad (6)$$

where f_{ci}, f_{cu} and f_{cr} are initial, ultimate and residual compressive strength respectively; G_{fch}, G_{fcs} and G_{fc} $(= G_{fch} + G_{fcs})$ are hardening, softening and total compressive fracture energy respectively. α is the configure parameter for the softening part of stress-plastic work curve.

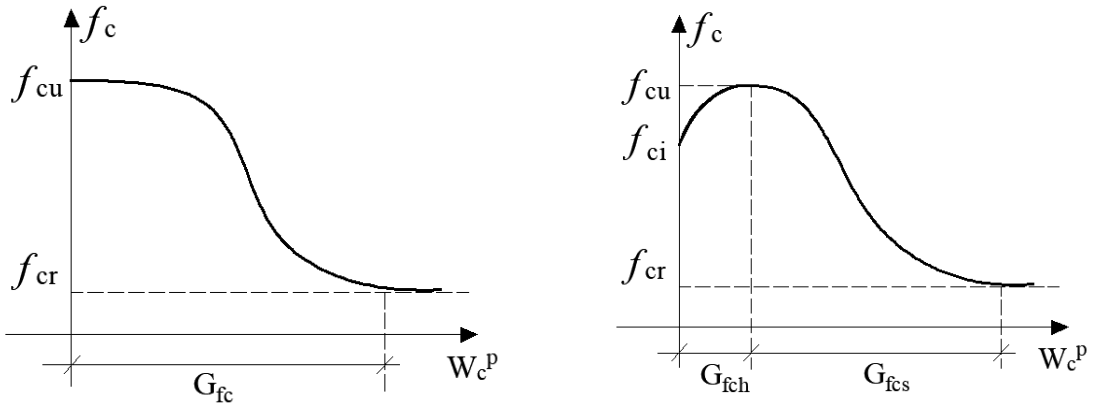

(a) (b)

Figure 3 Strength evolution of: (a) softening and (b) hardening-softening

Based on Eq. (6), the ratio of plastic work to fracture energies r_w can be written as:

$$r_w = \begin{cases} r_{ch} = \dfrac{W_c^p}{G_{fch}}, & W_c^p \le G_{fch} \\ r_{cs} = \begin{cases} \dfrac{W_c^p - G_{fch}}{G_{fcs}}, & G_{fch} < W_c^p \le G_{fc} \\ 1, & W_c^p > G_{fc} \end{cases} \end{cases} \tag{7}$$

Besides, the ratio of initial and residual strength to the ultimate strength are defined as:

$$\beta_i = \frac{f_{ci}}{f_{cu}}; \quad \beta_r = \frac{f_{cr}}{f_{cu}} \tag{8}$$

Substituting Eqs (7) and (8) into Eq (6), a damage parameter for the compressive failure can be expressed as:

$$D_c = \begin{cases} D_{ch} = (1-\beta_i)(1-2r_w + {r_w}^2), & W_c^p \le G_{fch} \\ D_{cs} = (1-\beta_r)[\alpha {r_w}^{\alpha-1} - (\alpha-1){r_w}^{\alpha}], & W_c^p > G_{fch} \end{cases} \tag{9}$$

And finally the strength is a function of damage parameters,

$$f_c = (1 - D_c) f_{cu} \tag{10}$$

In above equations, the softening damage parameter D_{cs} is controlled by the configure parameter α which helps to calibrate the geometry of polynomial curves as shown in Figure 4 where $f_{cu} = 20\ MPa,\ f_{cr} = 5\ MPa,\ G_{fc} = 0.5\ Nmm.$

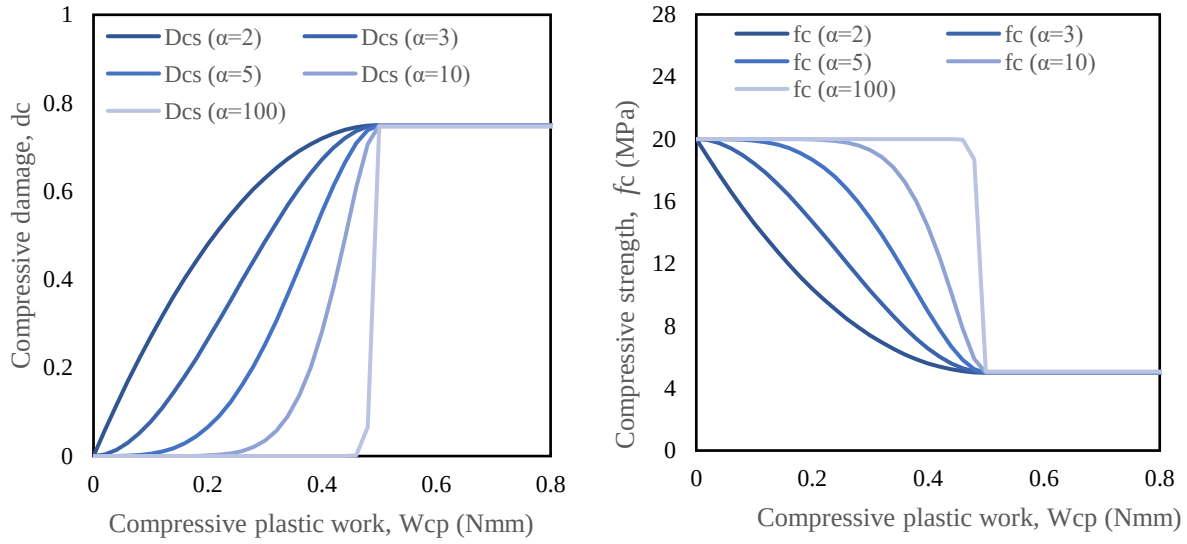

(a) (b)

Figure 4. Evolution of softening: (a) damage parameter D_{cs} and (b) compressive strength f_c

It should be noted that α should be no more than 2 to keep as a polynomial function.

3 Numerical implementation

An implicit backward Euler integration method is implemented in effective stress space and formulated in a monolithic form to determine the increment of plastic multiplier $d\lambda$ and the effective stress in current load step $\{\bar{\sigma}\}^{t+1}$ which is updated including elastic predictor (trial stress) and plastic corrector,

$$\{\bar{\sigma}\}^{t+1} = {}^{trial}\{\bar{\sigma}\}^{t+1} - d\lambda[K^0]\frac{\partial Q_c}{\partial\{\bar{\sigma}\}} \tag{11}$$

The trial stress is computed in an time incremental form considering the known effective stress in previous load step $\{\bar{\sigma}\}^t$ as well as deformation increment $\{du\}^{t+1}$.

$${}^{trial}\{\bar{\sigma}\}^{t+1} = \{\bar{\sigma}\}^t + [K^0]\{du\}^{t+1} \tag{12}$$

Integrating Eq (11) with Eq (3), a residual system is generated for Newton-Raphson (NR) iteration,

$$\{r\} = \begin{Bmatrix} \{r_\sigma\} \\ r_{d\lambda} \end{Bmatrix} = \begin{cases} \{\bar{\sigma}\}^{t+1} - {}^{trial}\{\bar{\sigma}\}^{t+1} + d\lambda[K^0]\dfrac{\partial Q_c}{\partial\{\bar{\sigma}\}} \\ F_c(\{\bar{\sigma}\}^{t+1}) \end{cases} \tag{13}$$

Different with Eq (3), the yield function $F(\{\bar{\sigma}\}^{t+1})$ in above system is not related with plastic work because the plasticity framework only updates effective stress and the increment of plastic multiplier, namely, a perfectly-plasticity concept is utilised in the effective stress space.

The gradient of the residual vector is a Jacobian matrix used for iteratively updating,

$$[\mathrm{J}] = \frac{\partial\{r\}}{\partial(\{\bar{\sigma}\}, d\lambda)} = \begin{bmatrix} [I] + d\lambda[K^0]\dfrac{\partial^2 Q_c}{\partial\{\bar{\sigma}\}^2} & [K^0]\dfrac{\partial Q_c}{\partial\{\bar{\sigma}\}} \\ \left(\dfrac{\partial F_c}{\partial\{\bar{\sigma}\}}\right)^{\mathrm{T}} & 0 \end{bmatrix} \tag{14}$$

After the completion of plasticity, the plastic work increment dW_c^p presented in the Eq.(4) can be rewritten by using the converged values as:

$$dW_c^p = d\lambda\{\bar{\sigma}\}^{\mathrm{T}}\{m\} \qquad \text{with} \qquad \{m\} = \begin{Bmatrix} m_n \\ m_s \end{Bmatrix} = \frac{\partial Q_c}{\partial\{\bar{\sigma}\}} \tag{15}$$

and then plastic work in current load step can be updated as $W_c^{p,t+1} = W_c^{p,t} + dW_c^{p,t+1}$ for calculating the damage parameter in current time step $D_c^{t+1} = D_c(W_c^{p,t+1})$. The procedure of the numerical implementation for the damage-plasticity model is listed in below algorithm which can be summarised by four stages: 1) transfer nominal stress to effective stress; 2) conduct elastoplastic update in effective stress space; 3) update the damage parameter; 4) transfer effective stress to nominal stress.

Algorithm. *Damage- plasticity interface model for the compressive model*

Given variables: $W^{p,t}$; $\{\sigma\}^t$; $\{du\}^{t+1}$; $[D]^t$
Effective stress: $\{\bar{\sigma}\}^t = ([I] - [D]^t)^{-1}\{\sigma\}^t$ and Trial stress: ${}^{trial}\{\bar{\sigma}\}^{t+1}$
Yield function with trial stress: ${}^{trial}F = F({}^{trial}\{\bar{\sigma}\}^{t+1})$
Elastic status:
IF $({}^{trial}F \le 0)$ **THEN**
    $\{\bar{\sigma}\}^{t+1} = {}^{trial}\{\bar{\sigma}\}^{t+1}$; $W^{p,t+1} = W^{p,t}$
    $[D]^{t+1} = [D]^t$; $\{\sigma\}^{t+1} = ([I] - [D]^{t+1})\{\bar{\sigma}\}^{t+1}$
Plastic status:
ELSE
    DO WHILE $(\|r\|^j > \mathrm{TOL})$
        $j = j + 1$
        Compute: $\{n\}^j; \{m\}^j; \left[\frac{\partial\{m\}}{\partial\{\bar{\sigma}\}}\right]; F^j$
        Jacobian $[\mathrm{J}]^j$ and its inverse matrix $([\mathrm{J}]^j)^{-1}$
        Residual vector $\{r\}^j$ and its norm: $\|r\|^j$
        Compute: $\begin{Bmatrix} \{\bar{\sigma}\}^{j+1} \\ d\lambda^{j+1} \end{Bmatrix} = \begin{Bmatrix} \{\bar{\sigma}\}^j \\ d\lambda^j \end{Bmatrix} - ([\mathrm{J}]^j)^{-1}\{r\}^j$
    ENDDO
    New effective stress: $\{\bar{\sigma}\}^{t+1} = \{\bar{\sigma}\}^j$
    Compute $dW^{p,t+1} = dW^p(\{\bar{\sigma}\}^j, \{m\}^j, d\lambda^j)$ and $W^{p,t+1} = W^{p,t} + dW^{p,t+1}$
    Update damage parameter: $[D]^{t+1} = [D](W^{p,t+1})$
    Compute nominal stress: $\{\sigma\}^{t+1} = ([I] - [D]^{t+1})\{\bar{\sigma}\}^{t+1}$
ENDIF

.

4 Numerical validation

To validate the proposed constitutive model in Section 2, the implementation algorithm in Section 3 is programmed as a user defined material subroutine (UMAT) for the finite element (FE) code Abaqus (version 6.14) which is powerful in analysing nonlinear problems. The interface model is implemented by using a 4-node cohesive element (COH2D4) which is fully restrained on the bottom edge and a displacement controlled load is applied vertically on the top edge. Modelling results are compared with the monotonic experimental result (specimen

named as *strong mortar*) from Kaushik et al (2007) and cyclic experimental result (specimen named as *B1*) from Oliveira et al (2006). Prisms with 5 clay bricks and 4 layer 10 mm thickness mortar joints tested by Kaushik et al (2007) and Oliveira et al (2006) are 400 mm and 280 mm height respectively. Material properties for the interface model are listed in Table 1. Others material parameters of all models are the same, including $C_{nn} = 1$, $C_{ss} = 9$ and $C_n = 0$. The convergence tolerance of the NR iteration is defined as 0.00001 with a maximum loop number 999 to avoid the endless iteration.

Table 1. Material properties of the proposed interface model.

Test units	K_n^0 N/mm^3	K_s^0 N/mm^3	G_{fch} N/mm	G_{fcs} N/mm	f_{ci} MPa	f_{cu} MPa	f_{cr} MPa	α
Monotonic Kaushik et al (2007)	40	20	7	8	2	7.5	1.5	3.5
Monotonic (Softening) Kaushik et al (2007)	10	5	-	11	-	7.5	1.5	5
Cyclic Oliveira et al (2006)	40	20	50	70	10	29	2	3.5
Cyclic (Softening) Oliveira et al (2006)	20	10	-	100	-	29	2	5

.

Numerical modelling results are compared with experimental results in Figure 5. The model only considers softening response (Figure 5a) has a good coincidence with the experimental result under monotonic loading because the stiffness deterioration of the specimen (*strong mortar*) is relatively light. However, the specimen (*B1*) under cyclic loading has a significant stiffness loss which cannot be properly predicted by the model only having the softening response. Besides, in the softening phase with unloading-reloading conditions, the stiffness degradation is overestimated by the model.

In Figure 5b, the modelling results predicted by the model with hardening/softening evolution have better consistency with the experimental results in terms of both strength variation and stiffness reduction. In the initial loading stage, the masonry prism has a high elastic stiffness that will gradually decrease during the loading process. To meet the good correlation in elastic-hardening stage, the normal elastic stiffness K_n^0 in model only with softening response has to be calibrated much lower than that in model with hardening/softening response, as listed in Table 1.

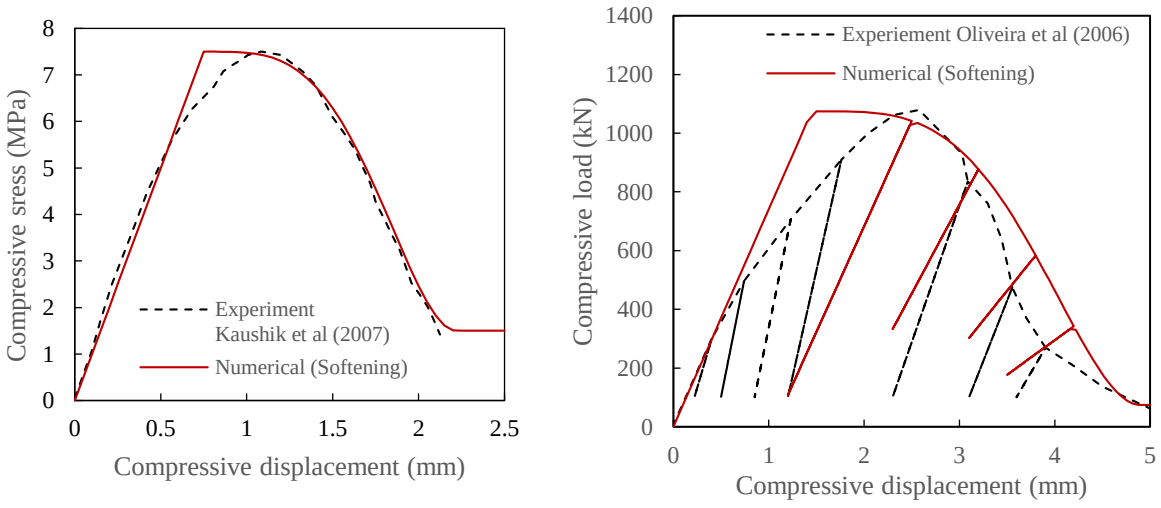

(a)

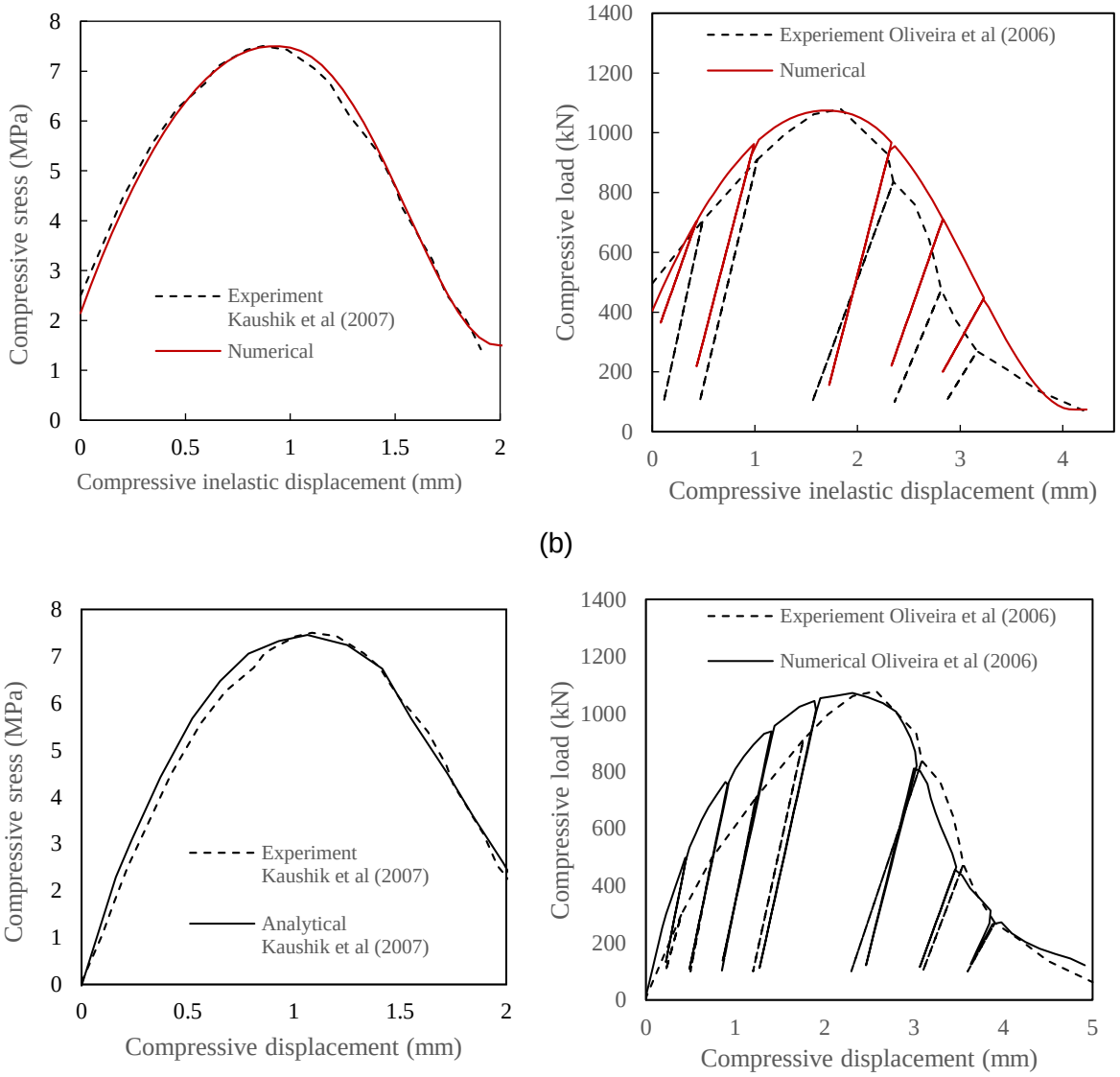

Figure 5. Comparison experimental results with numerical model (a) without hardening and (b) with hardening, and (c) other models from literatures

.

5 Conclusion

A damage-plasticity model is proposed for predicting the nonlinear response of masonry under monotonic and cyclic compressive loadings. The constitutive behaviour of the interface model is developed based on the traction-separation law in a 2D space which is commonly used in simplified micro-model for simulating the nonlinear behaviour of masonry structures. Compared with the plasticity model, the proposed model considering the effect of damage has capability to predict the stiffness degradation of masonry under the cyclic loading. Besides, the computational efficiency and robustness is greatly improved by introducing the damage parameter to control the softening response of the stress-displacement (relative) relations. Compared with the damage model, the inelastic deformation in present model can be calculated efficiently by using implicit integration method to prevent the overestimation of the stiffness degradation, which is an inevitable disadvantage existing in the pure damage model. To simplify the numerical implementation, damage and plasticity are decoupled algorithmically in nominal and effective stress spaces separately.

The evolution of the damage parameter along with the plastic work can be determined as either softening or hardening/softening expressions. All variables used in the proposed damage parameter equation have physical meanings except the configure coefficient α which is proposed to calibrate the shape of strength softening. In comparison with previous analytical equations from literatures, the proposed polynomial expression is a continuous curve which can be differentiated or integrated conveniently. Even though numerical modelling results illustrate that the concept of hardening/softening evolution can predict the nonlinear compressive behaviour of masonry prism better, it has shortcoming in implementing the elastoplastic part due to the perfectly-plasticity conception adopted in this study. In further work, improvement of the numerical implementation would be conducted by using hardening-plasticity conception.

6 References

Andreotti, G., Graziotti, F., & Magenes, G. (2018). Detailed micro-modelling of the direct shear tests of brick masonry specimens: the role of dilatancy. Engineering Structures, 168, 929-949.

Bui, T. T., Limam, A., & Sarhosis, V. (2021). Failure analysis of masonry wall panels subjected to in-plane and out-of-plane loading using the discrete element method. European Journal of Environmental and Civil Engineering, 25(5), 876-892.

Burton, C., Visintin, P., Griffith, M., & Vaculik, J. (2021, December). Laboratory investigation of pull-out capacity of chemical anchors in individual new and vintage masonry units under quasi-static, cyclic and impact load. In Structures (Vol. 34, pp. 901-930). Elsevier.

Calderón, S., Arnau, O., & Sandoval, C. (2019). Detailed micro-modeling approach and solution strategy for laterally loaded reinforced masonry shear walls. Engineering Structures, 201, 109786.

Derakhshan, H., Griffith, M. C., & Ingham, J. M. (2013). Out-of-plane behavior of one-way spanning unreinforced masonry walls. Journal of Engineering Mechanics, 139(4), 409-417.

Di Nino, S., & Luongo, A. (2019). A simple homogenized orthotropic model for in-plane analysis of regular masonry walls. International Journal of Solids and Structures, 167, 156-169.

Greco, F., Leonetti, L., Luciano, R., Pascuzzo, A., & Ronchei, C. (2020). A detailed micro-model for brick masonry structures based on a diffuse cohesive-frictional interface fracture approach. Procedia Structural Integrity, 25, 334-347.

Griffith, M. C., Vaculik, J., Lam, N. T. K., Wilson, J., & Lumantarna, E. (2007). Cyclic testing of unreinforced masonry walls in two ‐ way bending. Earthquake Engineering & Structural Dynamics, 36(6), 801-821.

Ingham, J., & Griffith, M. (2010). Performance of unreinforced masonry buildings during the 2010 Darfield (Christchurch, NZ) earthquake. Australian Journal of Structural Engineering, 11(3), 207-224.

Kaushik, H. B., Rai, D. C., & Jain, S. K. (2007). Stress-strain characteristics of clay brick masonry under uniaxial compression. Journal of materials in Civil Engineering, 19(9), 728-739.

Lotfi, H. R., and Shing, P. B. (1994). Interface model applied to fracture of masonry structures. Journal of structural engineering, 120(1), 63-80.

Lourenço, P. B., and Rots, J. G. (1997). Multisurface interface model for analysis of masonry structures. Journal of engineering mechanics, 123(7), 660-668.

Milani, G., Lourenço, P., & Tralli, A. (2007). 3D homogenized limit analysis of masonry buildings under horizontal loads. Engineering Structures, 29(11), 3134-3148.

Oliveira, D. V., Lourenço, P. B., & Roca, P. (2006). Cyclic behaviour of stone and brick masonry under uniaxial compressive loading. Materials and structures, 39(2), 247-257.

Sarhosis, V., & Lemos, J. V. (2018). A detailed micro-modelling approach for the structural analysis of masonry assemblages. Computers & Structures, 206, 66-81.

Smoljanović, H., Živaljić, N., Nikolić, Ž., & Munjiza, A. (2018). Numerical analysis of 3D dry-stone masonry structures by combined finite-discrete element method. International Journal of Solids and Structures, 136, 150-167.

Su, Y., Wu, C., & Griffth, M. C. (2011). Modelling of the bond–slip behavior in FRP reinforced masonry. Construction and Building Materials, 25(1), 328-334.

Vaculik, J., & Griffith, M. C. (2018). Out-of-plane shaketable testing of unreinforced masonry walls in two-way bending. Bulletin of Earthquake Engineering, 16(7), 2839-2876.